Development of a forest structural complexity index based on multispectral airborne remote sensing and topographic data[1]

Jon Pasher and Douglas J. King

Abstract: This paper presents development of a multivariate forest structural complexity index based on relationships between field-based structural variables and geospatial data. Remote sensing has been widely used to model individual forest structural attributes at many scales. As opposed to, or in addition to, individual structural parameters such as leaf area index or tree height, overall structural complexity information can enhance forest inventories and provide a variety of information to forest managers, including identifying damage and disturbance as well as indicators of habitat or biodiversity. In this study, a multivariate modelling technique, redundancy analysis, was implemented to derive a model incorporating both horizontal and vertical structural attributes as predicted by an ensemble of high-resolution multispectral airborne imagery and topographic variables. The first redundancy analysis axis of the final model explained 35% of the total variance of the field variables and was used as the complexity index. With a root mean squared error of 19.9%, the model was capable of differentiating four to five relative levels of complexity. This paper presents the forest ecological and modelling aspects of the research. A related paper presents the remote sensing aspects, including application of the model to map predicted structural complexity, map validation, and testing of the method at multiple scales.

Résumé : Cet article présente le développement d'un indice multivarié de complexité de la structure de la forêt basé sur les relations entre des variables structurales mesurées sur le terrain et des données géospatiales. La télédétection a été largement utilisée pour modéliser les attributs structuraux de la forêt à plusieurs échelles. Contrairement à, ou en plus, des paramètres structuraux individuels comme l'indice de surface foliaire ou la hauteur des arbres, une information globale au sujet de la complexité structurale peut améliorer les inventaires forestiers et fournir une variété de renseignements aux aménagistes forestiers, incluant l'identification des dommages et des perturbations aussi bien que des indicateurs d'habitat ou de biodiversité. Dans cette étude, une technique de modélisation multivariée, l'analyse de redondance, a été appliquée pour dériver un modèle qui incorpore des attributs, tant horizontaux que verticaux de la structure, prédits par un ensemble d'images aériennes multispectrales à haute résolution et des variables topographiques. Le premier axe de l'analyse de redondance du modèle final expliquait 35 % de la variance totale des variables terrain et a été utilisé comme indice de complexité. Avec une erreur quadratique moyenne de 19,9 %, le modèle était capable de différencier quatre à cinq niveaux de complexité. Cet article présente les aspects de la recherche reliés à la modélisation et à l'écologie forestière. Un autre article présente les aspects reliés à la télédétection, incluant l'application du modèle pour cartographier la complexité structurale prédite, la validation de la cartographie et l'essai de la méthode à plusieurs échelles.

[Traduit par la Rédaction]

Introduction

Understanding patch-level structural variations across a forest can enhance inventories and provide important information to forest managers. Specifically, information with respect to damage and disturbance (e.g., Cosmopoulos and King 2004; Wulder et al. 2008) as well as potential indicators of habitat or biodiversity (e.g., Winter et al. 2008; Pasher and King 2009) can be derived from horizontal and vertical structural information.

Remote sensing has been used for over two decades to model individual horizontal and vertical forest structural attributes at a variety of scales (e.g., Franklin and Strahler 1988; Cohen and Spies 1990). Specifically, structural attributes such as leaf area index (LAI), canopy closure, crown diameter, basal area, stem density, and tree heights have been the focus of most research. Modelling can involve image spectral and often spatial information, the latter usually in conjunction with very high-resolution sensor data. In the research presented here, airborne multispectral imagery was selected based on its generally low acquisition and processing costs for small coverage, its straightforward interpretation, and because this study follows on from the foundation of previous studies as described below. Other data have also

Received 12 January 2010. Accepted 9 September 2010. Published on the NRC Research Press Web site at cjfr.nrc.ca on 17 December 2010.

J. Pasher[2] and D.J. King. Department of Geography and Environmental Studies, Geomatics and Landscape Ecology Laboratory, Carleton University, 1125 Colonel By Drive, Ottawa, ON K1S 5B6, Canada.

[1]This article is one of a selection of papers from Extending Forest Inventory and Monitoring over Space and Time.
[2]Corresponding author (e-mail: jpasher@rogers.com).

been used successfully for forest structure modelling, including airborne synthetic aperture radar (SAR) (e.g., Breidenbach et al. 2008) and light detection and ranging (LiDAR) (e.g., Anderson et al. 2008).

Coops and Catling (1997*a*, 1997*b*) presented early research using remote sensing to model and map forest structural complexity as a multivariate construct. Using four band visible and near-infrared airborne videography with 2 m ground pixel size, they modelled eucalyptus forest habitat complexity as represented by an additive index of visual scores for canopy cover, shrub cover, ground vegetation cover, soil moisture, and debris (adapted from Newsome and Catling 1979). Using the same data set, Coops et al. (1998) refined the method by incorporating automated tree delineation to provide spectral and spatial statistics for individual tree crowns and crown clusters. Wunderle et al. (2007) used the first principal component of field-measured attributes (crown closure, crown diameter, overstorey and understorey species composition, overstorey diameter at breast height (DBH), heights, age, stem density, and basal area) as a structural complexity index in a boreal coniferous forest. It was then regressed against image variables extracted from pan-sharpened SPOT data (2.5 m panchromatic image fused with 10 m multispectral image). These studies are examples of structural indices that are predefined based on field ecological principles and data (see McElhinny et al. (2006), which presents a standardized methodology for such index development) and then modelled using remotely sensed data. In the following, studies are presented that have explored the relationships between remote sensing data and forest structure and, based on those relationships, developed a multivariate structure index for predictive mapping. They are representative of the approach taken in the research presented in this paper.

Olthof and King (2000) used canonical correlation analysis to examine linear relationships between multiple forest structural variables and image variables in a mixed boreal forest. Forest structure variables included crown closure, LAI, and live, standing dead, and fallen basal area. Image variables were derived from 50 cm pixel multispectral airborne digital camera data and included spectral brightness from within crowns and shadows as well as textural information. The first canonical variate was used as an image-based forest structure index. Cosmopoulos and King (2004) refined this methodology using regression of all image variables against the forest structure index and applying the resulting model in temporal mapping of forest structure change due to disturbance from nearby mining activities.

In a similar type of exploratory analysis, Sampson et al. (2001) used redundancy analysis (RDA), which is similar to a combined principal components analysis (PCA) and canonical correlation analysis and the focal method of this paper (see Modelling structural complexity using RDA section). They investigated relationships between forest structural variables (overstorey and understorey canopy openness, crown area, and basal area) and spectral indices calculated from hyperspectral airborne imagery to differentiate between three silviculture practices in a hardwood forest. Unfortunately, results were weak and dependent on the inclusion of clearcut plots with very high canopy openness. de la Cueva (2008) used RDA to differentiate forest types in western Spain through the derived relationships between structural variables (total vegetation closure, overstorey canopy closure, basal area, stem density, and stand height) and Landsat spectral variables and topographic data.

Research objectives

The primary objective of this research was to develop a multivariate structural complexity index in a temperate hardwood forest based on modelling the relationships between field-based structural variables and geospatial data. The geospatial data comprised variables extracted from high-resolution multispectral remotely sensed imagery and topographic information. Most past research has shown relationships between image texture or spatial dependence measures with composition or structural parameters, which vary horizontally over space. The current research advances this field of research by (*i*) examining structural modelling combining vertical and horizontal forest heterogeneity, (*ii*) incorporating multivariate information from both the imagery/topographic (predictor) and forest (predicted) data sets, and (*iii*) examining spatial information within individual canopy objects or spectrally defined fractions, such as the shadow fraction, to provide information on vertical structural heterogeneity. Since forest structure is inherently a multiscale concept, the image predictor variables used to explain field-based structural variations were extracted from multiple scales including at the overall plot scale and from individual objects information within the plots (i.e., individual tree crowns and canopy gaps).

Methods

Study area

The research was carried out in a small portion of Gatineau Park in southern Quebec. The selected study area (Fig. 1) was completely dominated (>99%) by hardwoods, with the dominant overstorey species being sugar maple (*Acer saccharum* Marsh.) and with small patches dominated by American beech (*Fagus grandifolia* Ehrh.), trembling aspen (*Populus tremuloides* Michx.), and red oak (*Quercus rubra* L.). Small numbers of red maple (*Acer rubrum* L.), basswood (*Tilia americana* L.), ironwood (*Ostrya virginiana* (Mill.) K. Koch), white ash (*Fraxinus americana* L.), black ash (*Fraxinus nigra* Marsh.), white birch (*Betula papyrifera* Marsh.), and black cherry (*Prunus serotina* Ehrh.) are also present. Being on the Canadian Shield, the topography is rolling with elevation variations of up to 300 m (King et al. 2005).

The study area was also selected where previous ice storm modelling and mapping had been carried out (King et al. 2005) as well as ongoing LAI modelling (Gonsamo et al. 2010). The ice storm combined with site characteristics (soil, drainage, and topography) have produced a diversity of horizontal and vertical forest structural conditions. The narrow rectangular shape of the study area was a direct consequence of the limited view angle of the airborne camera and the desire to minimize the number of flightlines.

Field data and structural measurements

In the summer of 2007, locations for 50 field plots were selected to represent the full range of structural and topo-

Fig. 1. Location of study area within the southern section of Gatineau Park near Ottawa, Ontario, Canada. Shown with 2005 SPOT satellite image in the background. (Courtesy P. Pellikka, University of Helsinki.)

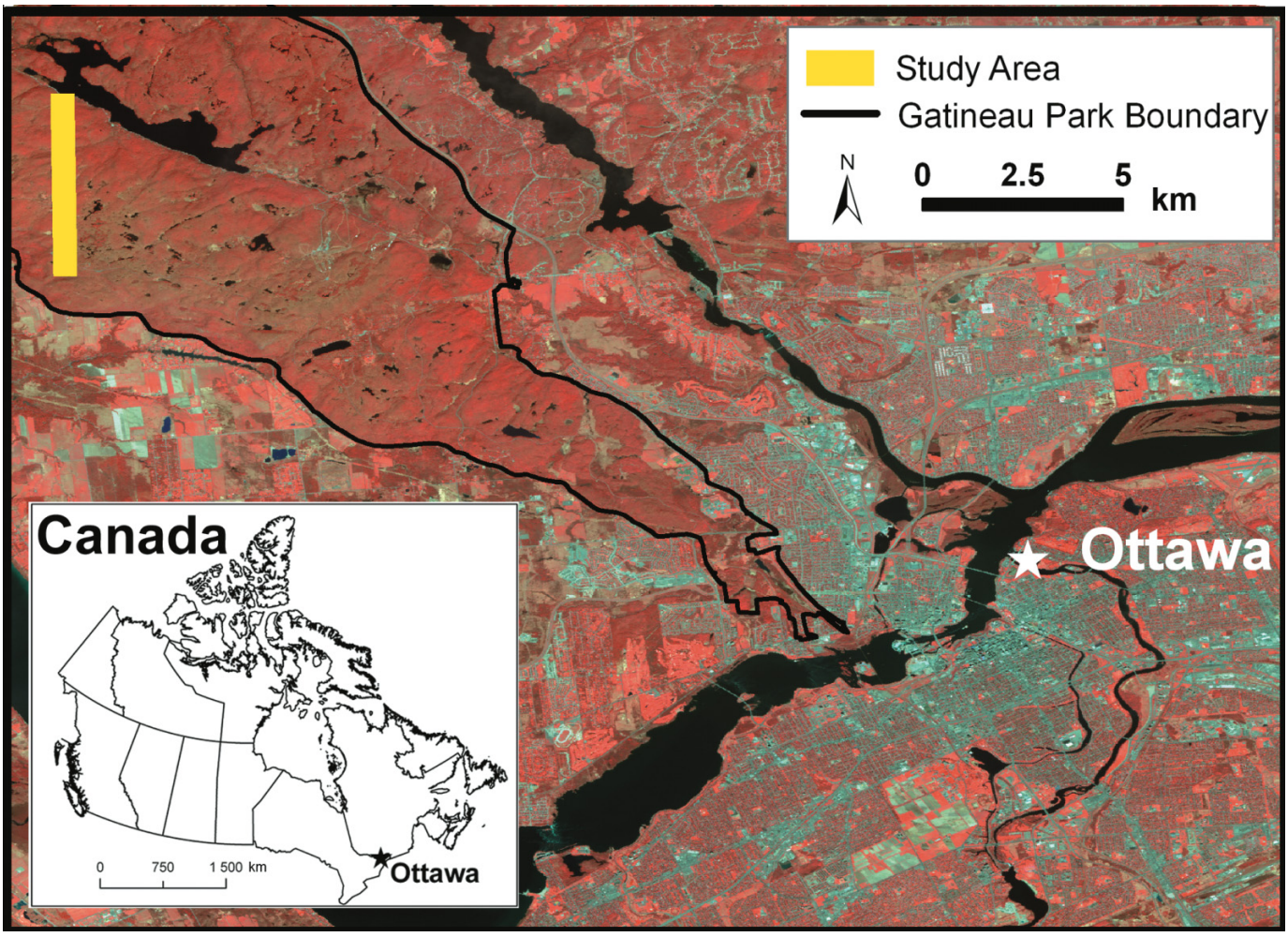

graphic conditions of the study area. The overstorey tree size and position, canopy closure, understorey and ground vegetation, and the amount of standing and fallen dead wood were qualitatively assessed before plot installation. The majority of plots were selected to have structural complexity in the middle portion of the range observed in the field. The remaining plots were split between areas with visually higher and lower structural complexity levels, which were known to be less frequently occurring and much smaller in size compared with medium-complexity areas.

At each location, a 20 m × 20 m field plot was established and the GPS position recorded. Plot size was chosen for continuity with previous forest structure research in the park (King et al. 2005) and based on optimal plot extent research for sample-based image analysis in this forest (Butson and King 2006). Field measurements taken in each plot were selected based on the literature as well as their expected manifestation in the imagery, either directly (e.g., crown size and canopy closure) or indirectly (e.g., large coarse woody debris that is not generally visible in the imagery but may be associated with overstorey gaps). Table 1 provides a summary of the field variables that were measured, which, as a group, represented the structural conditions in the plots.

Overstorey tree size and distribution

Overstorey trees (DBH > 10 cm at a height of 1.3 m) were measured in terms of presence, size, and horizontal distribution. These trees form the upper canopy and were expected to be visible in the imagery as well as directly influence the light conditions below. Each tree's DBH, height (using a clinometer), and crown diameter (major and minor perpendicular axes projected to ground level) were measured. Plot averages and standard deviations were calculated, the latter as a representation of tree size (DBH and crown diameter) variance and vertical stratification (height variance (Zenner 2000)). Additionally, the numbers of large living and dead (snags) trees were calculated as the number beyond the 90th size percentile (DBH > 35 cm) of all trees over all plots (N = 1055). Basal area was calculated by summing the individual basal area of all live trees in the plot and converting to units of square metres per hectare.

The average distance between trees was calculated, having been shown to be a useful horizontal structural indicator (Spies and Franklin 1991). More complicated indices such as the Clark–Evans index (Clark and Evans 1954) were not used, since indices are often difficult to interpret compared with simpler statistical measures calculated from the data distribution.

Table 1. Summary of field variables representing the various aspects of forest structural complexity that were measured in field plots (N = 50 plots).

Structural attributes	Variable	Minimum	Maximum	Average	SD
Overstorey tree (>10 cm DBH) number and size	Number of overstorey trees	5.00	42.00	21.10	9.29
	Average overstorey tree DBH (cm)	16.93	33.29	24.32	4.18
	SD of overstorey tree DBH (cm)	3.85	17.17	9.21	2.71
	Live basal area (m^2/ha)	8.17	47.26	25.99	7.30
	Number of large trees	0.00	6.00	2.14	1.63
	SD of overstorey tree height (m)	2.24	6.97	4.17	1.32
	Average overstorey crown diameter (m)	2.94	5.40	4.03	0.48
	SD of overstorey crown diameter (m)	0.07	2.82	1.15	0.41
Tree spacing	Average nearest-neighbour distance (m)	0.99	3.18	1.95	0.55
Vertical structure: canopy openness and LAI	1 m openness (0°–60°) (%)	1.00	14.50	6.01	3.82
	1 m LAI (55°–60°)	3.06	6.89	5.41	0.95
	6 m openness (0°–60°) (%)	3.30	45.50	15.61	8.77
	6 m LAI (55°–60°)	2.42	6.08	4.29	0.93
	Change in openness (0°–60°) (%)	–2.30	37.10	9.59	9.34
	Change in LAI (55°–60°)	–4.00	1.20	–1.12	1.28
Ground and understorey vegetation	0–10 cm ground vegetation (% of plot)	0.00	25.00	5.75	6.27
	10–50 cm ground vegetation (% of plot)	1.79	90.18	27.77	19.89
	50 cm – 1 m ground vegetation (% of plot)	0.00	33.04	6.68	6.52
	1–2 m ground vegetation (% of plot)	0.00	29.46	8.05	7.84
	>2 m ground vegetation (% of plot)	0.00	97.32	20.45	23.82
Snags and CWD (>7.5 cm diameter)	Number of snags	1.00	19.00	4.88	3.41
	Average snag DBH (cm)	11.97	49.34	22.88	7.68
	Dead basal area (m^2/ha)	0.30	19.15	5.49	4.10
	Number of pieces of CWD	1.00	30.00	12.14	6.86

Canopy openness and LAI

Canopy openness and LAI are common indirect measures of canopy structure (e.g., Frazer et al. 2000) that provide information related to productivity and light conditions in the forest, which impact the understorey and ground vegetation and can greatly affect stand structure and function (Canham 1988). Digital hemispherical photographs were taken in each plot using a Nikon Coolpix 8800 (8 MP) with an FC-E9 fisheye lens (180° field of view) under diffuse sky conditions. Photographs were taken at the plot centres to provide general measures of structure. Testing of the use of multiple photograph locations in low-, medium-, and high-complexity plots showed that a single photograph taken at the plot centre represented well the relative LAI and openness across the complexity gradient of the study. In addition, as some areas of low or high complexity were very localized, use of multiple photographs throughout plots in such areas would have included canopy of different vertical structure outside the plot but within the 55° view angle used for LAI extraction. An extendable pole was used to acquire photographs at heights of 1 and 6 m to provide additional vertical stratification information (Soudani et al. 2002). The hemispherical photographs were processed using DHP.exe (v. 4.5.2) and Tracwin.exe (v. 4.1.1) (Leblanc 2006) to calculate LAI using the CLX clumping index from hemispherical photographs (55°–60° zenith angle) (Leblanc et al. 2005). Canopy openness, or percent open sky (Frazer et al. 2000), was calculated using an integration of the gap fraction across the zenith angles from 0° to 60° (Miller 1967; S. Leblanc, personal communication (2008)).

Understorey and ground vegetation

In temperate hardwood forests, unless a major gap has been created that provides for penetration of direct sun irradiance, understorey and ground vegetation are generally not directly visible or measurable from airborne imagery. However, there is a direct connection between vegetation abundance and structure below the upper canopy with the overstorey structure in terms of canopy gaps and light penetration (Canham 1988). Therefore, understanding the vertical structure of the understorey can provide useful information contributing to the quantification of overall complexity (Spies and Franklin 1991). A line intercept method was used with a 50 cm sampling interval along the diagonals of the field plots (28 m length). Vegetation presence in five height classes was recorded: <10 cm (herbs and low grasses), 11–50 cm (ferns and tall grasses), 51 cm – 1 m (seedlings), 1–2 m (shrubs), and >2 m vegetation with DBH < 10 cm (following methods described for the same forest by Pisaric et al. 2008). The tallest vegetation present at each sample point was recorded, providing an overall understanding of vertical heterogeneity across the plots, as opposed to recording multiple heights at a single location.

Dead wood

Dead wood was measured in terms of snags and coarse woody debris (CWD). Snags >1.3 m in height were counted in each plot and their DBH and height were recorded to calculate average and standard deviation of snag size as well as dead basal area. CWD was sampled using the same line intercept method described above. The diameter of each piece of CWD that was >7.5 cm (Canadian Forest Inventory Committee 2004) and that intersected the line was recorded, permitting the tabulation of the number of pieces as well as the estimated volume of large CWD (Van Wagner 1964). Since the estimated volume was later found to be highly correlated with the number of pieces sampled, only the number of pieces was retained.

Airborne imagery acquisition and processing

Three-band CIR imagery (near-infrared, red, and green) was acquired just after solar noon over the study area on 21 August 2007 using a Duncantech Inc. MS4100 camera at a flight altitude of 650 m to achieve 20 cm nominal ground pixel size with a maximum view angle of 9.5°. This high resolution was selected to provide capability for delineation of tree crown objects and analysis of within-crown and within-shadow spectral and spatial information, which had been shown to be useful in forest structure modelling in previous research of the authors' research group (e.g., Lévesque and King 2003; Seed and King 2003). Spatial variations in brightness due to sun-sensor-surface geometry, specifically bidirectional reflectance variation, topography (slope and aspect in relation to subangle), and sensor-lens effects (Teillet et al. 1982; Pickup et al. 1995), were corrected using a net empirical correction (Pasher and King 2010). A mosaic of the images was then created and georeferenced to 2004 orthophotographs of 25 cm pixels (National Capital Commission 1998) using a thin plate exact fit spline with 38 control points. The root mean squared error (RMSE) for this procedure was approximately 3 m in both the X and Y directions or about 2% of the plot area.

Predictor/explanatory variables

A variety of image variables (Table 2) were derived for each field plot directly from the airborne imagery. Spectral information (image brightness, which is linearly related to reflectance), spatial information (variations in image brightness between pixels), and object (e.g., shadow and tree crown) information were extracted at multiple scales, including over the full plot, for individual objects, and from within objects. The average and standard deviations of these variables were calculated. The normalized difference vegetation index (NDVI) was retained as an image metric because, while it often saturates in areas of high LAI, it was expected to be sensitive to structure in lower LAI areas as well as within shadows. The percentage of each plot classified as canopy, shadow, and exposed wood was calculated from an ISODATA unsupervised clustering map (as in Seed and King 2003). Similarly, subpixel fractions of these three classes were calculated using linear spectral unmixing (as in Lévesque and King (2003) and Pasher et al. (2007)). Grey level co-occurrence matrix (GLCM) image texture (Haralick et al. 1973) was calculated using a 5 pixel × 5 pixel (1 m × 1 m) moving window. It was derived for the whole plot and separately for crown and shadow clusters. Increased texture within crowns was expected to be associated with increased crown openness and, in turn, increased understorey and ground vegetation abundance. Higher texture within shadows was expected to represent the presence of understorey vegetation and possible dead wood seen through canopy gaps. Semivariogram measures (range and sill), which have

Table 2. Summary of types of image variables extracted from multispectral airborne imagery that were used as predictors in modelling structural complexity.

Variable type	Variable	Variables extracted/derived
Spectral	Pixel level	% of plot classified (ISODATA unsupervised clustering) as vegetation, shadow, and exposed wood
		Mean and SD of near-infrared, red, green, and NDVI within each plot
		Variables calculated for full plots as well as for the vegetation and shadow components of the plot individually
	Subpixel	Mean and SD of fraction of sunlit crown, shadows, and exposed wood derived through linear spectral unmixing
Spatial	Image textures	Mean and SD of five texture measures calculated from the GLCM (Haralick et al. 1973) using a 5 × 5 window
		Variables calculated for full plot as well as for the vegetation and shadow components of the plot individually
	Semivariance	Range and sill from theoretical semivariogram of each spectral band
Object-based	Canopy and shadow objects	Number, mean, and SD of size of canopy objects in each plot (using tree delineation algorithm (Pouliot et al. 2005)) and area of shadow objects
		Mean and SD of shape complexity within each plot (deviation from circularity: Patton 1975)
Topographic		Elevation, slope, and aspect
		Solar illumination calculated at image acquisition time (Riano et al. 2003)

Note: With three spectral bands, there are multiple variables within each subcategory, with a final total of 86 image-based explanatory/predictor variables. The mean is the average calculated for all pixels in the sample. SD is the standard deviation calculated for all pixels in the sample.

been shown to be related to field-measured structural attributes (Treitz and Howarth 2000; Lévesque and King 2003), were calculated for each plot in each spectral band. Finally, as a potential indicator of crown size, horizontal tree distribution, and canopy openness, tree crowns and shadows were delineated as individual objects using an automated algorithm (Pouliot et al. 2005). The number and size distribution of these two types of objects were measured as well as measures of object shape complexity (Patton 1975), which were expected to increase in a more open and irregular overhead canopy.

Elevation, slope, and aspect as well as a measure of solar illumination (Riano et al. 2003) were derived from a digital elevation model with 10 m × 10 m cell size and a vertical RMSE of approximately 5.7 m (National Capital Commission 1998; Bemrose 2006).

Modelling structural complexity using RDA

The multivariate nature of forest structural complexity, remotely sensed data, and topographic data lends itself well to multivariate statistical techniques designed to explore relationships between multiple predictors and response variables. RDA, which can be thought of as a PCA of multivariate regression predicted values (Stewart and Love 1968; Legendre and Legendre 1998), is an excellent statistical tool for this type of analysis. In a simplified manner, an RDA is carried out by calculating multiple linear regressions for each response variable (y) individually (in this case the field variables) followed by a single PCA of the fitted/predicted response variables (y'). The resultant components, or canonical axes, which are uncorrelated and represent decreasing proportions of the original variance in the set of response variables, can then be interpreted in terms of their relationship to the original field variables (similar to examining factor loadings in a PCA) and the explanatory/predictor variables that were included in the model (Legendre and Legendre 1998).

A two-stage RDA was carried out using bootstrapping for variable selection and model validation. A linear response between explanatory and response variables was assumed following tests for unimodality, which examined the gradient length, described in ter Braak and Šmilauer (2002). It could be hypothesized that certain field variables, such as canopy openness, would exhibit unimodal relationships with certain image variables. For example, both an extremely open and closed canopy would result in homogeneity in the imagery, while heterogeneity in the imagery would be seen with intermediate closure in the canopy. However, since only half of the full distribution of potential values (canopy openness ranged from 3.3% to 45.5%) existed in these data, they were approximated using a linear relationship.

As summarized in Fig. 2, a two-stage RDA procedure was programmed in Matlab incorporating existing code from Peres-Neto et al. (2006) and Jones (2008) (R. Proulx, personal communication (2008)). In the first stage, 500 iterations of the RDA using forward stepwise selection were run, each time randomly selecting 40 of the 50 field plots and resulting in 500 models. This ensured that variable selection was not solely dependent on the set of input data used. In the second stage, these models were individually tested by running each through an RDA, this time not using stepwise selection but instead entering only those variables that were selected in the first stage. This second stage was also bootstrapped, running 500 iterations and selecting 40 out of 50 plots each time. However, at each iteration, the 10 field plots that were withheld were used to validate the model, with cumulative statistics recorded over the second round of 500 iterations. The average adjusted R^2 and the average Akaike information criterion were summarized for each model. The predicted first RDA axis ($RDA_{predicted}$) was calculated by applying the RDA model to the set of image variables of the 10 validation plots. $RDA_{predicted}$ represented the predicted canonical axis produced from a linear combination of predictor (i.e., image and topographic) variables.

Fig. 2. RDA modelling process showing two-stage bootstrapping.

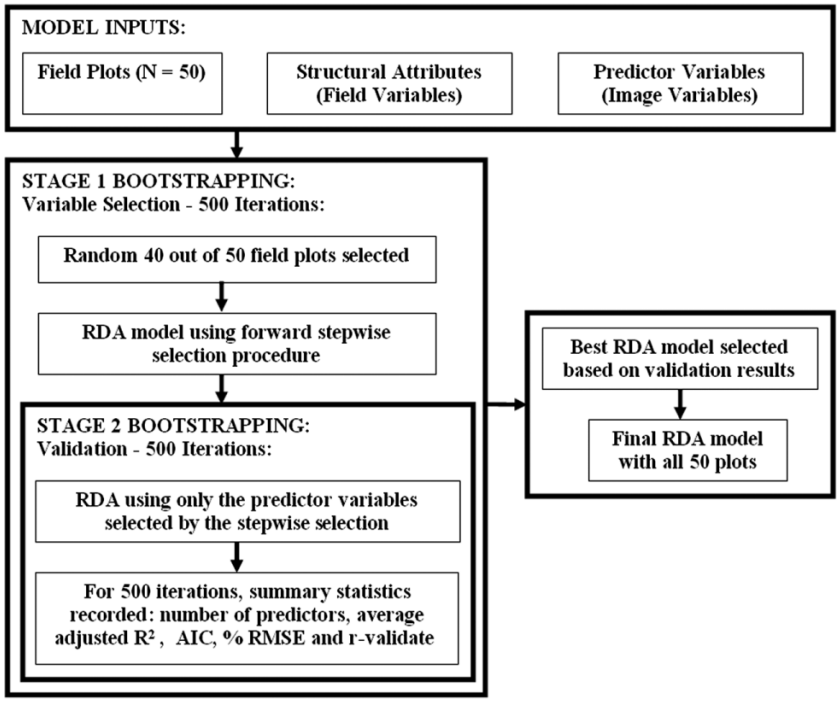

It was then directly compared with the corresponding variate calculated using the observed information ($RDA_{observed}$) from the 24 field variables measured in each of the 10 plots. Therefore, similar to validating multiple regression models, only with multiple dependent variables instead of a single one, a predicted *y* variable ($RDA_{predicted}$) and an observed *y* variable ($RDA_{observed}$) were calculated. Since the RDA produced canonical axes that were in a different projected space from the original data, the observed field variables were first transformed into the equivalent projected space as the modelled canonical axes using a transformation matrix (the U matrix (Legendre and Legendre 1998)). The correlation (referred to from this point on as "*r*-validate") and the RMSE (% RMSE of the range of actual RDA values) between $RDA_{predicted}$ and $RDA_{observed}$ were then calculated and the average values were derived from the 500 iterations for each model. The models were ranked from best to worst based on the validation statistics and the top models were selected for further evaluation. The final selected RDA model was processed using CANOCO 4.5 (ter Braak and Šmilauer 2002), which provided the desired numerical and graphical outputs.

Results

Field plot structural conditions

Ten field plots were qualitatively identified as having relatively low structural complexity, while 11 had relatively high complexity. Both of these conditions were less common throughout the study area than the structural conditions of the remaining plots. These divisions were subjective and qualitative and not used for any quantitative analysis, but they served as a means to visually classify and understand the structural differences between plots. Low structural complexity was generally represented by homogeneous overstorey, no ground vegetation or continuous low ground vegetation, and very little to no CWD (Figs. 3A and 3B). High structural complexity typically included large canopy gaps, variable overstorey tree sizes, and significant amounts of CWD, often in piles, mixed with variable ground and understorey vegetation (Figs. 3C and 3D). This was reflected in large differences in the hemispherical photographs and resulting canopy openness and LAI measurements for the 1 and 6 m heights (Fig. 4). Table 1 shows summary statistics for each of the attributes. Skewed variables were individually transformed prior to being used for modelling.

RDA modelling and development of a structural complexity index

Bootstrapping resulted in 500 models that provided a range of explained variance of the field variables and included a range of predictor variables (Table 3 provides summary statistics of the models). The RDA models included between one and 14 predictor variables (mean = 3.12) with adjusted R^2 values from 0.17 to 0.48 (mean = 0.29). The best three models, based on the results from validation in the second-stage RDA bootstrapping analysis, had nine predictor variables, which was deemed to be too many given that there were only 50 field plots in the model. The fourth through seventh ranked models included the same six predictor variables (adjusted R^2 = 0.40, RMSE = 20%) in order of contribution to the model: (1) within-crown standard deviation of GLCM homogeneity, (2) within-crown average GLCM correlation, (3) green band semivariogram range, (4) the number of delineated canopy objects, (5) standard deviation of green band shadow brightness, and (6) incoming solar radiation. From a practical perspective, since the semivariogram is computationally intensive to calculate for every pixel across the image to apply such a model to produce a continuous map, and since semivariogram range was

Fig. 3. Structural conditions typical of area of relatively low structural complexity (A (Plot 2) and B (Plot 35)) and relatively high structural complexity (C (Plot 43) and D (Plot 12)) within the study area.

correlated with many other variables ($r > 0.6$), it was decided to select the next (eighth) ranked model that did not include semivariogram measures. It included five variables, three being the same as variables 1, 2, and 5 listed above. The other two variables entered were the average within-shadow NDVI and elevation. This model and the relationships of these five variables with structural complexity are described below.

The selected model, processed for all 50 plots together (CANOCO output in Table 4), had an adjusted R^2 of RDA1 = 0.35 ($p < 0.001$). The second RDA axis provided a further 6% explanation; however, it was not highly significant ($p = 0.080$) and as discussed later was not of particular interest. The first axis was defined as a structural complexity index (SCI), as it represented a multivariate structural complexity gradient. The average RMSE for the model, derived through bootstrapping, was 19.9%.

An examination of the biplot scores (Table 5) showed that standard deviation of within-crown GLCM homogeneity (IM1) and the average within-crown GLCM correlation (IM2) were positively correlated with SCI and that increasing complexity within tree crowns, caused by dead or thin branches and small gaps in the crowns, manifested itself as greater variation in crown reflectance (texture and texture variation across the crown). SCI was positively correlated with within-shadow average NDVI (IM3) relating to the presence of vegetation within canopy gaps at heights just below the upper canopy. SCI was negatively correlated with within-shadow texture (standard deviation of the green band, or IM4), again potentially showing a gradient of increased shadow homogeneity caused by an increasing density of vegetation within the gaps. This variable provided little contribution to the SCI and was difficult to interpret and was potentially included in the RDA simply as a suppressor variable. Finally, elevation (IM5) was positively correlated with SCI, although it provided very little contribution to the axis. It is a similar topographic variable to solar illumination ($r = 0.40$, $p = 0.004$), although it is less complex. At higher elevations in the study area, it was evident that overstorey trees were generally smaller in height and crown size, resulting in a more open canopy with increased light suitable for understorey and ground vegetation growth. Conversely, the SCI showed that complexity increased with increasing average overstorey DBH along with increasing canopy openness. Generally speaking, canopy openness showed a greater impact on complexity compared with tree size, and although not highly significant, the second RDA axis, which was predominantly composed of elevation variance ($r = 0.73$, $p < 0.001$), showed that at increasing elevations, the average crown size and overstorey DBH decreased and canopy openness increased.

Figure 5 presents the triplot created for the selected model using CanoDraw (ter Braak and Šmilauer 2002). It provided various types of information, including the information previously presented by the image biplot scores. The five predictor variables (IM1–IM5) are displayed as red arrows with their length and direction relative to SCI (RDA1 on the *X*-axis) indicative of their contribution to the SCI. Each field variable ($N = 24$) is displayed as a blue arrow; field variables positively correlated with one another are drawn close to each other (e.g., number of overstorey trees and live basal area; $r = 0.60$, $p < 0.001$). Arrows that point in opposite directions are negatively correlated (e.g., number of overstorey trees and average crown diameter; $r = –0.46$, $p < 0.001$) and arrows that approach right angles to one another are not correlated (e.g., number of overstorey trees and

Fig. 4. Example binarized hemispherical photographs (white areas are gaps) taken in a plot with relatively low complexity (Plot 2) (L) as well as a plot with relatively high complexity (Plot 20) (H). Large differences between the 1 and 6 m photographs can be seen in the high-complexity plot as a result of the thick understorey vegetation (H-1m) and the large canopy gaps (H-6m). The opposite was generally true in the low-complexity plots where little understorey vegetation was present to block the camera lens (L-1m) and few significant canopy gaps existed (L-6m).

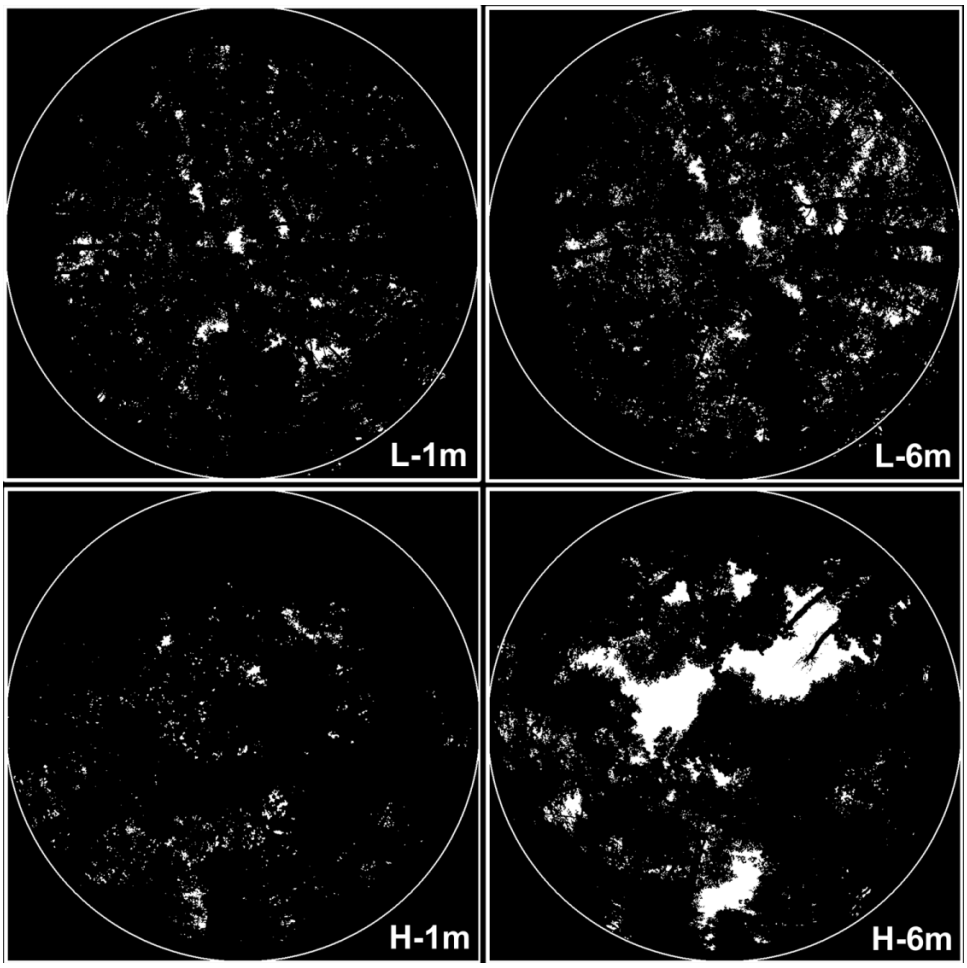

Table 3. Summary statistics calculated from the 500 models (all $p < 0.001$) that were produced from the first phase of bootstrapping in RDA, which was carried out for variable selection.

	Adjusted R^2	*r*-validate	Number of predictors	% RMSE	Akaike information criterion
Average	0.29	0.69	3.12	25.6	349.4
Minimum	0.17	0.60	1.00	17.6	344.7
Maximum	0.48	0.83	14.00	38.3	361.5

Note: Statistics calculated for each of the 500 models were used to rank models and select a final model for further evaluation.

Table 4. Summary results from final RDA model (produced by CANOCO).

	Axis				
Axis variance	1	2	3	4	Total
Eigenvalue	0.35	0.06	0.02	0.01	1.00
Field-image correlation	0.81	0.67	0.50	0.33	
Cumulative percent variance of field data	34.5	40.6	42.6	43.7	
Cumulative percent variance of field-image relationship	77.7	91.6	95.9	98.5	
Sum of all eigenvalues					1.00
Sum of all canonical eigenvalues					0.44
Test of significance of first canonical axis	Eigenvalue = 0.35, $F = 23.17$, $P < 0.001$				

Table 5. RDA biplot scores for predictor variables in the final RDA model.

Variable	Predictor variable	RDA biplot score
IM1	Variation of within-crown texture (GLCM homogeneity)	0.86
IM2	Average within-crown texture (GLCM correlation)	0.42
IM3	Average within-shadow NDVI	0.30
IM4	SD within-shadow of green band	–0.19
IM5	Elevation	0.10

Note: Scores show the relative importance of each predictor variable towards RDA1 and the sign of each shows the relative direction compared with RDA1.

Fig. 5. Triplot for the final RDA model. The first axis (*X*-axis) represents the SCI showing a gradient of structural complexity in the forest, and the second axis (*Y*-axis) represents slight structural variations related mainly to changes in elevation (IM5). The red vectors represent image and topographic predictor variables ($N = 5$) and the blue arrows represent each field variable ($N = 24$). The 50 field plots are shown as coloured dots representing initial visual field classification (green, low complexity; orange, moderate complexity; red, high complexity). Their position relative to the *X*-axis represents their modelled level of structural complexity.

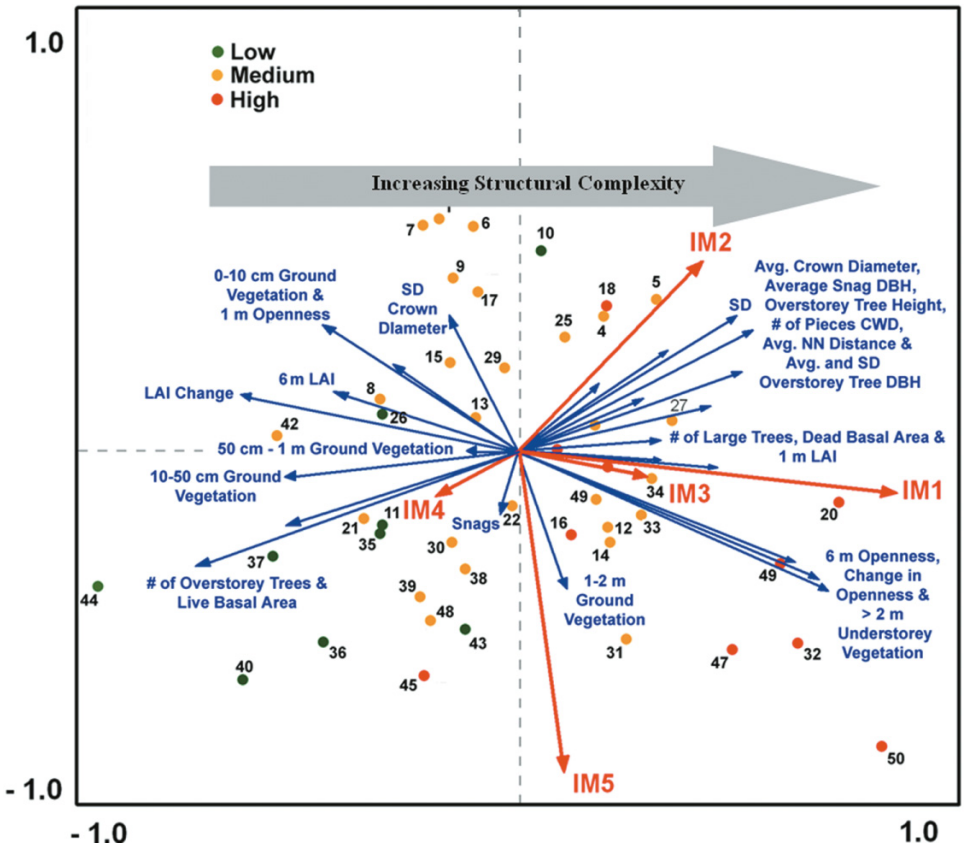

standard deviation of crown diameter; $r = 0.01$, $p = 0.963$). Similarly, relationships between field variables (blue arrows) and predictor variables (red arrows) can be inferred based on the directions of the arrows. For example, IM3, representing vegetation within canopy gaps, is positively correlated with LAI at 1 m height ($r = 0.34$, $p = 0.018$) and understorey vegetation at >2 m height ($r = 0.33$, $p = 0.018$), both represented by arrows close to IM3.

Finally, the triplot displays the 50 field plots based on their RDA score on each axis. From left to right along the *X*-axis, the structural complexity of the plots increases. Additionally, the field plots can be examined in terms of individual structural attributes. For example, Plots 37, 40, and 44, which were predicted to have low structural complexity, had among the highest number of overstorey trees, while Plot 50 with high predicted structural complexity had relatively few overstorey trees, which were of variable sizes (DBH and height), large canopy gaps, and abundant understorey vegetation (covering 97.3% of the plot). The field plots are shown in Fig. 5 with colours reflective of the preliminary qualitative classification that was assigned to each plot when they were established. For the most part, plots assessed as relatively low (green dots) or high (red dots) complexity were predicted to have low or high SCI values, respectively. This is shown in a simplified manner in Fig. 6 where the original three qualitative classes (*Y*-axis) are plotted against the RDA-predicted SCI score (*X*-axis). This figure confirmed that most low- and high-complexity plots were distinguishable but that there was a small amount of overlap with medium-complexity plots.

Fig. 6. Relationship between the modeled SCI (*X*-axis) shown using a standardized scale from lowest SCI (–2.7) to highest SCI (2.3) and the initial visual field classification by complexity level. Field plots that showed confusion between classes are circled for each complexity class (i.e., low, medium, and high).

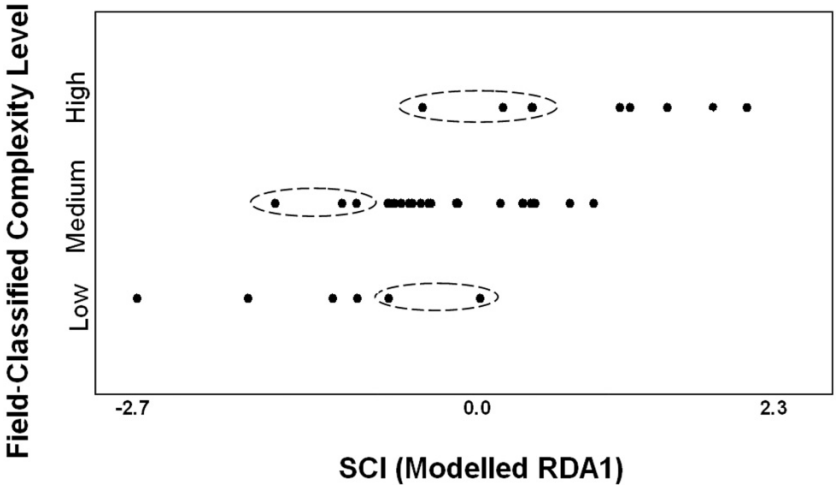

Visual analysis of the triplot provided a summary of the SCI, but an examination of the signs of the bivariate correlations between SCI and the individual field variables (i.e., the field variable biplot scores used to define the arrows on the triplot) shown in Table 6 provided additional explanation. From this table, it can be seen that increasing structural complexity was associated with (*i*) increasing canopy openness, increasing understorey vegetation (>2 m), and decreasing low ground vegetation (0–50 cm), (*ii*) increasing size of overstorey trees (average DBH), greater numbers of large trees, fewer overstorey trees, and decreasing live basal area, and (*iii*) larger snags (average snag DBH), more dead basal area, and more CWD pieces.

Discussion

Development of an SCI

While the first RDA axis (SCI) provided explanation for only 35% of the variance in the field data, it was never expected to be used to predict actual values of the individual field variables but instead to represent the general multivariate gradient of structural complexity. Potential sources for the unexplained variance include measurement error and the inherent randomness associated with a natural system. The topographic variables represented the general light regime and macrosite characteristics; however, microsite characteristics that are known to be related to damage susceptibility and regeneration were not included. Soil type, depth, and rockiness, which are known to affect the structure of forests (e.g., Diaci and Boncina 2005; Schmoeckel and Kottmeier 2008), were not included in the analysis, since these variables were not thought to manifest themselves directly or indirectly in the imagery. Structural variations beneath the canopy were not expected to be completely manifested in the imagery, since understorey radiance exiting through the canopy is mostly evident only in gaps between trees where understorey vegetation is immediately below the overstorey layer. As well, while the camera view angle was relatively narrow (9.5°), the solar zenith angle at the time of acquisition was greater (33.7°). Understorey vegetation that is below the overhead canopy is often in areas adjacent to overhead gaps where sunlight penetrates the canopy at the given solar zenith and azimuth angles. Thus, its radiance may not be directly evident in the imagery within gaps. The use of LiDAR data to provide vertical canopy structure and a bare earth elevation model could potentially help to overcome such issues.

A variety of field-based structural indices have been developed to quantify and differentiate levels of forest structural complexity. Subjectively scored indices, such as that presented by Newsome and Catling (1979), do not require intensive field data collection; however, their repeatability is limited. Similarly, additive indices based on field measurements, such as the 18-attribute index of Van Den Meerschaut and Vandekerkhove (1998), often rely on subjective weights for each structural attribute in the index. Other indices such as those presented by Zenner (2000), Staudhammer and LeMay (2001), and Pommerening (2002) were designed with silvicultural practices in mind, particularly related to stand growth and development. These indices are constructed using only a few structural attributes, usually related to overstorey tree size and distribution, and do not include information about dead wood or understorey and ground vegetation. McElhinny et al. (2006) developed an index without subjective weights that combined 13 structural attributes, including overstorey, understorey, ground vegetation, and dead wood information. All of the above methods for deriving a field-based index have benefits but they are limited to point- or plot-based sampling across a forest. Their potential for mapping with remote sensing may also be constrained if the field attributes selected for the index do not contribute to radiance exiting the canopy (e.g., proportions of rock and litter in relatively closed canopies). Remotely sensed imagery provides spatially extensive data and development of an SCI based on the multivariate relationships between image and field attributes provides greater potential for mapping complexity over a given area. However, such an index may have reduced sensitivity to ground vegetation conditions.

Table 6. Correlation coefficients (and biplot scores) between field variables and SCI (first RDA axis) shown to strongest to weakest (the empty row divides significant from nonsignificant correlations).

Field variable	Pearson *r*	*p*
Number of overstorey trees	–0.72	<0.001
Change in openness (0°–60°) (%)	0.70	<0.001
>2 m ground vegetation (% of plot)	0.67	<0.001
Change in LAI (55°–60°)	–0.63	<0.001
6 m openness (0°–60°) (%)	0.62	<0.001
Average snag DBH (cm)	0.53	<0.001
10–50 cm ground vegetation (% of plot)	–0.52	<0.001
Live basal area (m^2/ha)	–0.51	<0.001
Average nearest-neighbour distance (m)	0.50	<0.001
SD of overstorey tree height (m)	0.49	<0.001
1 m LAI (55°–60°)	0.45	<0.001
0–10 cm ground vegetation (% of plot)	–0.43	0.002
Average overstorey tree DBH (cm)	0.43	0.002
6 m LAI (55°–60°)	–0.41	0.003
Number of pieces of CWD	0.34	0.017
Dead basal area (m^2/ha)	0.32	0.022
Number of large trees	0.32	0.025
1 m openness (0°–60°) (%)	–0.28	0.051
SD of overstorey tree DBH (cm)	0.28	0.052
Average overstorey crown diameter (m)	0.18	0.211
50 cm – 1 m ground vegetation (% of plot)	–0.12	0.423
1–2 m ground vegetation (% of plot)	0.11	0.461
SD of overstorey crown diameter (m)	–0.05	0.735
Number of snags	–0.04	0.782

The results presented here were considered successful compared with similar RDA-type modelling studies using remote sensing, with the SCI explaining approximately 35% of the variance in the field-collected structural information. In comparison, Sampson et al. (2001), using only spectral information extracted from hyperspectral airborne imagery in hardwood forests, did not produce useful relationships with respect to developing a gradient of complexity. Their modelling rested solely on the canopy openness variable and the relationship was lost altogether when clearcut plots were removed. Olthof and King (2000), followed by Cosmopoulos and King (2004), used a pseudo-RDA analysis to derive a forest structure index that provided approximately 26% and 28% explanation of the original field data, respectively. Finally, de la Cueva (2008), using spectral (albeit lower spatial resolution Landsat) and topographic information, found a maximum of 24% explanation when combining both the first and second RDA axes.

RDA methods have some significant advantages over other SCI methods. Multicollinearity of field attributes was not a major issue, and therefore, the inclusion of multiple response (field) variables accounting for some of the same variance does not matter. Within RDA, the dimensionality is reduced using PCA, and therefore, multiple correlated field variables, for example as shown by clustered structural attributes (blue arrows) in Fig. 5, are reduced to a single vector. Consequently, preprocessing of field variables (e.g., as in McElhinny et al. 2006) to produce an uncorrelated core variable set is not required. The methods presented relating field-based structural complexity to image variables utilized raw field data measured in a set of field plots. Since this type of raw information is readily available in forest inventory plots, no further information, or processing of that information, is required.

Interpretation of the SCI from an ecological perspective

The bivariate correlations between the field variables and SCI (Table 5) allowed the SCI to be interpreted in terms of its representation of field-based structural complexity. Increased understorey vegetation resulting from increased canopy openness and light penetration (Canham 1988) provided vertical heterogeneity in certain study plots. This was predominantly from maple saplings that have benefited from canopy damage caused by the 1998 ice storm. Pisaric et al. (2008) showed that plots in Gatineau Park that experienced greater ice storm damage generally showed little increase in ground vegetation below 50 cm height in the 2 years following the storm. These results are supported in this research, which showed more complex plots to have less low ground vegetation, most likely due to shading from saplings that grew quickly following the storm.

Higher structural complexity was also represented by increased amounts of dead wood (increasing snag DBH and number of pieces of CWD). The benefits of both standing dead trees and woody debris on the forest floor in terms of providing habitat and increasing biodiversity are well known. However, not surprisingly, the actual number of snags in the field plots was uncorrelated with SCI (r = –0.04, p = 0.782). The number of pixels representing snags within each plot was very small and therefore probably not

well represented in the plot-based image variables. As well, many of these snags were created 9 years earlier in the severe ice storm of 1998. The surrounding vegetation structure had changed significantly in the intervening years, creating a disconnect between the presence of snags and many of the other variables. As a result, snags did not appear to be a main contributor, although they are certainly important structures. The number of snags was also not well correlated with other field variables that were not measures of dead wood ($|r|_{average}$ = 0.21, $|r|_{maximum}$ = 0.48). This finding provided justification for associated research investigating the detection and mapping of snags as a separate habitat indicator (Pasher and King 2009), which could be integrated with the SCI presented here.

Interestingly, five of the 24 field variables were found to be uncorrelated with the SCI (Table 5). Crown diameter measurements were known to have significant error due to the measurement methods (tests showed ~14% coefficient of variation). Another variable, 1–2 m ground vegetation, was positively correlated with the second RDA axis; however, that axis was not found to be highly significant. While only providing a small amount of explanation, the second RDA axis did show that some structural variance was explained by elevation. This supported existing research showing greater ice storm damage, and therefore greater complexity, at higher elevations in Gatineau Park (King et al. 2005).

Application of results and future research

This research presents methods for developing an image-based SCI that could be used as an indicator of disturbance, habitat, and biodiversity. The two RDA error measures, RMSE (19.9%) and the proportion of plots (82%) well distinguished as high or low structural complexity (Fig. 6), indicate that this modelling procedure could be used to accurately identify and target areas of high or low structural complexity for further field assessment or for monitoring of disturbance and major structural changes over time. Structural complexity as an indicator of biodiversity can be integrated into forest inventory (e.g., Winter et al. (2008) using inventory plot data) and conservation management. Using a remote sensing approach, potential for mapping structural complexity and associated biodiversity value is increased.

The index and models developed are associated directly with the imagery used and therefore are not meant to be spatially extended to other areas unless field and image conditions are consistent. Instead, the methods for modelling structural complexity could be used to develop similar relationships and information in new areas. As well, the methods and results presented in this manuscript are not intended for coarse-scale mapping and monitoring programs but rather for local (patch) scale forest management. A full analysis of the impact of changing scale up to 1 m pixels on the SCI models and mapping accuracy showed that the contributions of the various types of spatial information in such images decline at coarser scales but that some are still significant (Pasher and King 2010); this would not be the case for moderate-resolution data such as Landsat. An ongoing project developed following the completion of this research is investigating these aspects (Torontow and King 2010). It is being conducted over a larger area with Quickbird imagery (1 m panchromatic pixels and 2.5 m multispectral pixels) in more mixed wood conditions and it is comparing image modelling of direct field-based indices derived using the methods of McElhinny et al. (2006) with the RDA image-based modelling methods of this paper. Preliminary results show that both types of methods are capable of producing useful models for structural–compositional complexity modelling.

The inclusion of other sources of information such as LiDAR data, which have been shown to be very useful for extracting three-dimensional forest structural information (e.g., Lim et al. 2003; Anderson et al. 2008), could potentially increase the strength of the SCI modelling. Of particular interest to this research was the work by Anderson et al. (2008), which modelled forest structural parameters (albeit individual parameters and not a multivariate forest representation) using LiDAR in a northern temperate forest. They compared the use of airborne hyperspectral data in combination with LiDAR with the use of each data set on its own. Results showed that for six structural parameters examined, the average adjusted R^2 values increased from 0.26 (LiDAR) and 0.32 (hyperspectral) to 0.42 when the two data types were used together. Such results suggest that while LiDAR data could be very important for forest structural modelling, image information may be as or more important and should not be dismissed. While LiDAR data are becoming increasingly affordable, collection over small areas is more expensive compared with airborne or satellite multispectral imagery. Further research comparing and combining multispectral and LiDAR data will be conducted in the Gatineau Park, as LiDAR data were acquired in 2010.

Conclusions

This research contributes to ongoing efforts to develop remote sensing based methods to enhance field-based measurement and monitoring of forest structural variations. While most remote sensing based forest structure research has focused on modelling individual horizontal and vertical structural attributes, this research presented methods for exploring and modelling forest structure as a multivariate construct. The use of high-resolution remotely sensed data and RDA modelling is a new approach for measuring structural complexity across a forest. The method relies on relationships between measured field data and image or topographic data to drive the model rather than predefining a field-based index and trying to model it with remote sensing data. While the study was conducted in a temperate hardwood forest in southern Quebec, the methods are applicable to other forest types. Modelling multivariate structural complexity within a forest using a set of field plots and geospatial information, including both remotely sensed imagery and topographic information, would permit forest managers to map local structural complexity variations across the entire forest. This can provide information related to damage and disturbance as well as information related to habitat and biodiversity, which is increasingly becoming of great interest to forest practitioners responsible for forest inventories (e.g., Winter et al. 2008). With forests being managed to maintain, if not enhance, complexity, this type of information, especially spatially across the forest, is extremely valuable (Larson 2007).

Acknowledgements

This research was funded by a Natural Sciences and Engineering Research Council of Canada Discovery Grant to D.J. King. The Canada Foundation for Innovation, the Ontario Innovation Trust, the National Wildlife Research Centre, and private sources funded Carleton University's Geomatics and Landscape Ecology Laboratory, which provided all of the necessary field equipment and data processing infrastructure used in this research. The authors are grateful to the National Capital Commission for access to Gatineau Park and for providing geospatial data used in this research. Many thanks to C. Czerwinski for his extensive help in the field as well as M. Leni, V. Torontow, and R. Bemrose. The continuous feedback and advice of I. Olthof (Canada Centre for Remote Sensing), E. Humphreys (Department of Geography and Environmental Studies, Carleton University), and J. Kerr (Department of Biology, University of Ottawa) has been greatly appreciated. Many thanks to N. Walsworth, D. Patterson, and E. Seed for technical support. Finally, the intensive RDA modelling support and advice of R. Proulx (currently at the University of Québec, Trois Rivières) are greatly appreciated.

References

Anderson, J.E., Plourde, L.C., Martin, M.E., Braswell, B.H., Smith, M.-L., Dubayah, R.O., Hofton, M.A., and Blair, J.B. 2008. Integrating waveform Lidar with hyperspectral imagery for inventory of a northern temperate forest. Remote Sens. Environ. **112**(4): 1856–1870. doi:10.1016/j.rse.2007.09.009.

Bemrose, R.K. 2006. Impacts of radiometric corrections on empirical modelling of biophysical variables with airborne multispectral digital camera imagery. M.Sc. thesis, Department of Geography and Environmental Studies, Carleton University, Ottawa, Ont.

Breidenbach, J., Koch, B., Kandler, G., and Kleusberg, A. 2008. Quantifying the influence of slope, aspect, crown shape and stem density on the estimation of tree height at plot level using Lidar and InSAR data. Int. J. Remote Sens. **29**(5): 1511–1536. doi:10.1080/01431160701736364.

Butson, C.R., and King, D.J. 2006. Lacunarity analysis to determine optimum extents for sample-based spatial information extraction from high-resolution forest imagery. Int. J. Remote Sens. **27**(1): 105–120. doi:10.1080/01431160500238844.

Canadian Forest Inventory Committee. 2004. Canada's National Forest Inventory — ground sampling guidelines version 4.1, 13 February 2004 [online]. Available at https://nfi.nfis.org/documentation/ground_plot/Gp_guidelines_v4.1.pdf [accessed 1 August 2009].

Canham, C.D. 1988. An index for understorey light levels in and around canopy gaps. Ecology, **69**(5): 1634–1638. doi:10.2307/1941664.

Clark, F.J., and Evans, F.C. 1954. Distance to the nearest neighbour as a measure of spatial relationships in populations. Ecology, **35**(4): 445–453. doi:10.2307/1931034.

Cohen, W.B., and Spies, T.A. 1990. Remote sensing of canopy structure in the Pacific Northwest. Northwest Environ. J. **6**: 415–418.

Coops, N.C., and Catling, P.C. 1997*a*. Predicting the complexity of habitat in forests from airborne videography for wildlife management. Int. J. Remote Sens. **18**(12): 2677–2682. doi:10.1080/014311697217530.

Coops, N.C., and Catling, P.C. 1997*b*. Utilising airborne multispectral videography to predict habitat complexity in eucalypt forests for wildlife management. Wildl. Res. **24**(6): 691–703. doi:10.1071/WR96099.

Coops, N.C., Culvenor, D., Preston, R., and Catling, P.C. 1998. Procedures for predicting habitat and structural attributes in eucalypt forests using high spatial resolution remotely-sensed imagery. Aust. For. **61**(4): 244–252.

Cosmopoulos, P., and King, D.J. 2004. Temporal analysis of forest structural condition at an acid mine site using multispectral digital camera imagery. Int. J. Remote Sens. **25**(12): 2259–2275. doi:10.1080/0143116032000160507.

de la Cueva, A.V. 2008. Structural attributes of three forest types in central Spain and Landsat ETM plus information evaluated with redundancy analysis. Int. J. Remote Sens. **29**(19): 5657–5676. doi:10.1080/01431160801891853.

Diaci, J.R.P., and Boncina, A. 2005. Regeneration in experimental gaps of subalpine *Picea abies* forest in the Slovenian Alps. Eur. J. For. Res. **124**(1): 29–36.

Franklin, J., and Strahler, A.H. 1988. Invertible canopy reflectance modeling of vegetation structure in semiarid woodland. IEEE Trans. Geosci. Remote Sens. **26**(6): 809–825. doi:10.1109/36.7712.

Frazer, G.W., Trofymow, J.A., and Lertzman, K.P. 2000. Canopy openness and leaf area in chronosequences of coastal temperate rainforests. Can. J. For. Res. **30**(2): 239–256. doi:10.1139/cjfr-30-2-239.

Gonsamo, A., Pellikka, P.K.E., and King, D.J. 2010. Large scale leaf area index inversion algorithms from high resolution airborne imagery. Int. J. Remote Sens. In press.

Haralick, R.M., Shanmugam, K., and Dinstein, I. 1973. Textural features for image classification. IEEE. Trans. Syst. Man Cybernet. **3**(6): 610–621. doi:10.1109/TSMC.1973.4309314.

Jones, D. 2008. FATHOM: A Matlab toolbox for ecological and oceanographic data analysis [online]. Available at http://www.rsmas.miami.edu/personal/djones/matlab/matlab.html [accessed 1 August 2009].

King, D.J., Olthof, I., Pellikka, P.K.E., Seed, E.D., and Butson, C. 2005. Modelling and mapping forest ice storm damage using remote sensing and environmental data. Nat. Hazards, **35**(3): 321–342. doi:10.1007/s11069-004-1795-4.

Larson, B.C. 2007. Thoughts on the development of new, appropriate measures of complexity. IUFRO Forest Research Information Paper 167: Complex stand structures and associated dynamics — measurement indices and modelling approaches, 29 July – 2 August, Sault Ste. Marie, Ont.

Leblanc, S.G. 2006. Digital hemispherical photography manual v. 1.3b. Canadian Centre for Remote Sensing, Natural Resources Canada, Ottawa, Ont.

Leblanc, S.G., Chen, J.M., Fernandes, R., Deering, D.W., and Conley, A. 2005. Methodology comparison for canopy structure parameters extraction from digital hemispherical photography in boreal forests. Agric. For. Meteorol. **129**(3–4): 187–207. doi:10.1016/j.agrformet.2004.09.006.

Legendre, P., and Legendre, L. 1998. Numerical ecology. 2nd English ed. Elsevier Science BV, Amsterdam, The Netherlands.

Lévesque, J., and King, D.J. 2003. Spatial analysis of radiometric fractions from high-resolution multispectral imagery for modelling individual tree crown and forest canopy structure and health. Remote Sens. Environ. **84**(4): 589–602. doi:10.1016/S0034-4257(02)00182-7.

Lim, K., Treitz, P., Baldwin, K., Morrison, I., and Green, J. 2003. Lidar remote sensing of biophysical properties of tolerant hardwood forests. Can. J. Remote Sens. **29**(5): 658–678.

McElhinny, C., Gibbons, P., and Brack, C. 2006. An objective and

quantitative methodology for constructing an index of stand structural complexity. For. Ecol. Manag. **235**(1–3): 54–71. doi:10.1016/j.foreco.2006.07.024.

Miller, J.B. 1967. A formula for average foliage density. Aust. J. Bot. **15**(1): 141–144. doi:10.1071/BT9670141.

National Capital Commission. 1998. Digital elevation data for Gatineau Park. National Capital Commission, Ottawa, Ont.

Newsome, A.E., and Catling, P.C. 1979. Habitat preferences of mammals inhabiting heathlands of warm temperate coastal, montane and alpine regions of southeastern Australia. *In* Ecosystems of the world. Vol. 9A. Heathlands and related shrublands of the world. *Edited by* R.L. Specht. Elsevier, Amsterdam, The Netherlands. pp. 301–316.

Olthof, I., and King, D.J. 2000. Development of a forest health index using multispectral airborne digital camera imagery. Can. J. Remote Sens. **26**(3): 166–176.

Pasher, J., and King, D.J. 2009. Mapping dead wood distribution in a temperate hardwood forest using high resolution airborne imagery. For. Ecol. Manag. **258**(7): 1536–1548. doi:10.1016/j.foreco.2009.07.009.

Pasher, J., and King, D.J. 2010. Multivariate forest structure modelling and mapping using high resolution airborne imagery and topographic information. Remote Sens. Environ. **114**(8): 1718–1732. doi:10.1016/j.rse.2010.03.005.

Pasher, J., King, D.J., and Lindsay, K. 2007. Modelling and mapping potential hooded warbler (Wilsonia citrina) habitat using remotely-sensed imagery. Remote Sens. Environ. **107**(3): 471–483. doi:10.1016/j.rse.2006.09.022.

Patton, D.R. 1975. A diversity index for quantifying habitat edge. Wildl. Soc. Bull. **3**(4): 171–173.

Peres-Neto, P.R., Legendre, P., Dray, S., and Borcard, D. 2006. Variation partitioning of species data matrices: estimation and comparison of fractions. Ecology, **87**(10): 2614–2625. doi:10.1890/0012-9658(2006)87[2614:VPOSDM]2.0.CO;2. PMID: 17089669.

Pickup, G., Chewings, V.H., and Pearce, G. 1995. Procedures for correcting high resolution airborne video imagery. Int. J. Remote Sens. **16**(9): 1647–1662. doi:10.1080/01431169508954502.

Pisaric, M.F.J., King, D.J., MacIntosh, A.J.M., and Bemrose, R. 2008. Impact of the 1998 ice storm on the health and growth of sugar maple (*Acer saccharum* Marsh.) dominated forests in Gatineau Park, Quebec. J. Torrey Bot. Soc. **135**(4): 530–539. doi:10.3159/08-RA-053R.1.

Pommerening, A. 2002. Approaches to quantifying forest structures. Forestry, **75**(3): 305–324. doi:10.1093/forestry/75.3.305.

Pouliot, D.A., King, D.J., and Pitt, D.G. 2005. Development and evaluation of an automated tree detection–delineation algorithm for monitoring regenerating coniferous forests. Can. J. For. Res. **35**(10): 2332–2345. doi:10.1139/x05-145.

Riano, D., Chuvieco, E., Salas, J., and Aguado, I. 2003. Assessment of different topographic corrections in Landsat-TM data for mapping vegetation types. IEEE Trans. Geosci. Remote Sens. **41**(5): 1056–1061. doi:10.1109/TGRS.2003.811693.

Sampson, P.H., Treitz, P.M., and Mohammed, G.H. 2001. Remote sensing of forest condition in tolerant hardwoods: an examination of spatial scale, structure and function. Can. J. Rem. Sens. **27**(3): 232–246.

Schmoeckel, J., and Kottmeier, C. 2008. Storm damage in the Black Forest caused by the winter storm "Lothar" — Part 1: Airborne damage assessment. Nat. Hazards Earth Syst. Sci. **8**(4): 795–803. doi:10.5194/nhess-8-795-2008.

Seed, E.D., and King, D.J. 2003. Shadow brightness and shadow fraction relations with effective LAI: importance of canopy closure and view angle in mixedwood boreal forest. Can. J. Remote Sens. **29**(3): 324–335.

Soudani, K., Trautmann, J., and Walter, J.M.N. 2002. Leaf area index and canopy stratification in Scots pine (*Pinus sylvestris* L.) stands. Int. J. Remote Sens. **23**(18): 3605–3618. doi:10.1080/01431160110110983.

Spies, T.A., and Franklin, J.F. 1991. The structure of natural young, mature, and old-growth Douglas-fir forests in Oregon and Washington. *In* Wildlife and vegetation of unmanaged Douglas-fir forests. *Edited by* K.B. Aubry, M.H. Brookes, J.K Agee, R.G. Anthony, and J.F. Franklin. U.S. For. Serv. Gen. Tech. Rep. PNW-GTR-285. pp. 91–109.

Staudhammer, C., and LeMay, V.M. 2001. Introduction and evaluation of possible indices of stand structural diversity. Can. J. For. Res. **31**(7): 1105–1115. doi:10.1139/cjfr-31-7-1105.

Stewart, D., and Love, W.A. 1968. A general canonical correlation index. Psychol. Bull. **70**(3 pt.1): 160–163. doi:10.1037/h0026143. PMID:5681306.

Teillet, P.M., Guindon, B., and Goodenough, D.G. 1982. On the slope-aspect correction of multispectral scanner data. Can. J. Remote Sens. **8**(2): 84–106.

ter Braak, C.J.F., and Šmilauer, P. 2002. CANOCO reference manual and CanoDraw for Windows. user's guide: Software for Canonical Community Ordination (v. 4.5). Microcomputer Power, Ithaca, N.Y.

Torontow, V.A., and King, D.J. 2010. Multivariate forest modeling and mapping using Quickbird imagery and topographic data in Chelsea, Québec. Proceedings of the Prairie Summit: 31st Canadian Symposium on Remote Sensing — The Prairie Summit, 1–6 June 2010, Regina Sask. Canadian Association of Geographers, Canadian Cartographic Association, Canadian Geomorphology Research Group, and Canadian Remote Sensing Society. pp. 309–312.

Treitz, P.M., and Howarth, P.J. 2000. High spatial resolution remote sensing data for forest ecosystem classification: an examination of spatial scale. Remote Sens. Environ. **72**(3): 268–289. doi:10.1016/S0034-4257(99)00098-X.

Van Den Meersschaut, D., and Vandekerkhove, K. 1998. Development of a stand scale forest biodiversity index based on the State Forest Inventory. *In* Integrated tools for natural resources inventories in the 21st century. *Edited by* M. Hansen and T. Burk. U.S. For. Serv. Gen. Tech. Rep. NC-212. pp. 340–349.

Van Wagner, C.E. 1964. The line intersect method in forest fuel sampling. For. Sci. **14**(1): 20–26.

Winter, S., Chirici, G., McRoberts, R.E., Hauk, E., and Tomppo, R. 2008. Possibilities for harmonizing national forest inventory data for use in forest biodiversity assessments. Forestry, **81**(1): 33–44. doi:10.1093/forestry/cpm042.

Wulder, M.A., White, J.C., Coops, N.C., and Butson, C.R. 2008. Multi-temporal analysis of high spatial resolution imagery for disturbance monitoring. Remote Sens. Environ. **112**(6): 2729–2740.

Wunderle, A.L., Franklin, S.E., and Guo, X.G. 2007. Regenerating boreal forest structure estimation using SPOT-5 pan-sharpened imagery. Int. J. Remote Sens. **28**(19): 4351–4364. doi:10.1080/01431160701244849.

Zenner, E.K. 2000. Do residual trees increase structural complexity in Pacific Northwest coniferous forests? Ecol. Appl. **10**(3): 800–810. doi:10.1890/1051-0761(2000)010[0800:DRTISC]2.0.CO;2.